Journal of Integrative Neuroscience

J. Integr. Neurosci. **2026**; 25(1): 46638
https://doi.org/10.31083/JIN46638

Original Research

Overexpression of IL7R Attenuates Cerebral Ischemia–Reperfusion Injury by Inhibiting Apoptosis

Shiqi Yang[1,2,3], Qian Su[1], Wenting Liu[1], Delong Meng[1], Zhiqiang Su[1,*]

[1]Department of Neurology, First Affiliated Hospital of Harbin Medical University, Harbin Medical University, 150001 Harbin, Heilongjiang, China
[2]Department of Neurology, Fourth Affiliated Hospital of Harbin Medical University, Harbin Medical University, 150001 Harbin, Heilongjiang, China
[3]Key Laboratory of Acoustic, Optical and Electromagnetic Diagnosis and Treatment of Cardiovascular Diseases, 150001 Harbin, Heilongjiang, China
*Correspondence: suzhiqiang2025@163.com (Zhiqiang Su)

Academic Editor: Hahn Young Kim
Submitted: 16 September 2025 Revised: 4 November 2025 Accepted: 11 November 2025 Published: 9 January 2026

Abstract

Background: Cerebral ischemia-reperfusion injury (CIRI) represents the most critical pathological event in the evolution of ischemic stroke (IS). Apoptosis is particularly important in CIRI pathophysiology. The interleukin-7 receptor (IL7R) is involved in various disease regulatory mechanisms; however, its specific role during CIRI remains unclear. We investigated the mechanistic function of IL7R in CIRI through a mouse model *in vivo* and through an astrocyte model *in vitro*. **Methods**: C57BL/6 mice were randomly allocated to one of five groups: (1) sham; (2) transient middle cerebral artery occlusion (tMCAO); (3) tMCAO + IL7R treatment; (4) tMCAO + negative control (NC); or (5) tMCAO + IL7R + the phosphatidylinositol 3-kinase (PI3K) pathway inhibitor (LY294002) (n = 3–7 per group) to evaluate the role of IL7R in CIRI. The *in vitro* study groups were (1) control; (2) oxygen-glucose deprivation/reoxygenation (OGD/R); (3) OGD/R + IL7R; (4) OGD/R + NC; and (5) OGD/R + IL7R + LY294002 groups. After IL7R overexpression was induced, the resulting changes in infarct volume, neurological score, cell viability, and expression of apoptosis-related proteins were assessed. **Results**: IL7R overexpression significantly attenuated CIRI-induced apoptosis. *In vivo*, this intervention improved neurological function, alleviated cerebral edema, and decreased infarct volume in tMCAO mice. *In vitro*, after the overexpression of IL7R, flow cytometry analysis revealed a reduction in apoptosis rates post-OGD/R, whereas transmission electron microscopy revealed fewer morphological alterations associated with apoptosis. In addition, the level of Bcl-2-associated X protein (Bax) and cysteine-dependent aspartate-specific Protease-3 (caspase-3) were decreased, whereas that of B-cell lymphoma-2 (Bcl-2) was increased; these effects were reversed by LY294002. **Conclusion**: Overexpression of IL7R was shown to alleviate CIRI by suppressing apoptosis. These findings indicate IL7R as a novel target for IS treatment.

Keywords: apoptosis; IL7R; ischemic stroke; PI3K/Akt; reperfusion injury

1. Introduction

Cerebrovascular diseases rank as one of the leading global causes of mortality [1]. Ischemic stroke (IS), an aggressive and widespread subtype of acute stroke [2]. After ischemia, the resulting restoration of blood supply can paradoxically worsen brain damage, a condition called cerebral ischemia–reperfusion injury (CIRI). CIRI is implicated in relatively high rates of mortality and disability, greatly influencing both the health of individuals and their quality of life [3,4]. Given its high incidence, the underlying mechanisms of CIRI remain elusive. The induction of apoptosis is a key event in CIRI. The reactive oxygen species (ROS) are rapidly produced after ischemia initiates the processes of neuronal death, brain edema, and subsequent cellular damage [5]. During reperfusion, ROS and oxidative stress (OS) can even cause the apoptosis of cells, aggravating brain damage [6]. Hence, suppressing OS and inhibiting apoptosis are essential measures to improve CIRI outcomes, indicating the need to search for possible treatment targets.

Interleukin-7 (IL-7) is a cytokine of four antiparallel alpha-helices that bind to cytokine receptors known as type I cytokine receptors. Stromal cells constitute the primary source of IL-7. IL-7 is necessary for the ontogeny and maintenance of lymphocytes [7], with a role in immune system homeostasis [8]. IL-7 acts by using the IL-7 receptor (IL7R), which is a heterodimeric protein comprising an α-chain (IL7Rα, also called CD127) and a γ-chain [9]. IL7R is involved in several pathological conditions, including autoimmune diseases and malignancies [10]. *IL7R*, as a protein-coding gene, is involved in cytokine-receptor activity and antigen binding [11] and orchestrates lymphocyte development through multiple convergent signaling cascades [12,13]. Specifically, the phosphatidylinositol 3-kinase (PI3K)/protein kinase B (Akt) pathway is implicated in CIRI and has neuroprotection [14]. In a recent study, IL7R was shown to be involved in disease states such as immunodeficiency and multiple sclerosis [15], and its downstream signaling cascades are well elucidated [16]. IL-7 has been found to regulate the process of autophagy in lung carcinoma cells by activating the PI3K/Akt pathway [17].

IL-7/IL7R signaling has also been shown to be involved in preventing apoptosis in human non-small cell lung cancer (NSCLC) by varying B-cell lymphoma-2 (Bcl-2) and Bax through the p53 pathway [18]. In subarachnoid hemorrhage, temporal differences in IL-7 expression in astrocytes were found to differ between patients with good and poor outcomes [19]. Despite these findings, the relationship between IL7R and CIRI remains unexplored. Considering the documented involvement of IL7R in apoptotic regulation and PI3K/Akt pathway activation across various pathologies, we propose that IL7R could suppress neuronal cell death through this signaling axis, consequently attenuating CIRI manifestations.

Stroke, a prevalent neurological disorder with substantial global health implications, continues to demand innovative treatment solutions. The present study proposed an innovative therapeutic strategy for IS through the modulation of IL7R expression. Through *in-vivo* and *in-vitro* experiments, elevated IL7R expression mitigates CIRI was revealed through the suppression of apoptosis, which is mediated by PI3K/Akt signaling pathway activation. These results establish IL7R as a viable candidate for developing targeted interventions against CIRI.

2. Materials and Methods

2.1 Animals

The study design complied with the Animal Research: Reporting of *In Vivo* Experiments (ARRIVE) guidelines [20]. Male C57BL/6 mice, ranging in weight from 20 to 25 g, were used for this investigation. All Specific Pathogen Free (SPF)-grade mice were obtained from Liaoning Changsheng Biotechnology Co., Ltd. (Benxi, Liaoning, China) and were maintained by animal-care protocols established by the First Affiliated Hospital of Harbin Medical University. Throughout the study, the mice were housed under strictly regulated conditions with a 12/12-h photoperiod and an ambient temperature maintained at 23–25 °C. Under anesthesia, the mice were kept at a constant 37 °C. Mice were randomly assigned to the following groups: (1) sham; (2) transient middle cerebral artery occlusion/reperfusion (tMCAO/R); (3) tMCAO/R + negative control (NC); (4) tMCAO/R + IL7R; and (5) tMCAO/R + IL7R + the PI3K pathway inhibitor (LY294002). A total anesthetic and analgesia were administered during every surgical procedure. The detailed grouping criteria and the mice that died or bled are already provided in the **Supplementary Table 1, Experiment 1–3**.

2.2 Intracerebroventricular Injection of Recombinant Adeno-Associated Virus (rAAV)

Hanheng Biological Technology (Shanghai, China) Co., Ltd. supplied the AAV serotype 9 expressing IL7R (AAV-IL7R; Titer: 1.5×10^{12} vector genome/mL; Promoter: CMV, 87012638) used in this research. The transfection efficiency was assessed with an AAV encoding green fluorescent protein (AAV-GFP; Titer: 1.3×10^{12} vector genome/mL, 87012636, Hanheng Biological Technology). The negative control was AAV-null (87012637, Hanheng Biological Technology), which is devoid of IL7R encoding. Each mouse was given a 2 µL intraventricular injection of the viral suspension three weeks before tMCAO induction. The lateral ventricle was injected with AAV-IL7R, AAV-GFP, or AAV-null 21 days before tMCAO induction. The experimental groups were chosen at random. The mice were prepared by shaving their heads and disinfecting them under anesthesia (1.25% avertin, JT0781, Jitian Biotechnology Co., Ltd., Beijing, China, i.p.). The mice were fasted for 4 h before anesthesia to prevent any incidents during the procedure. Core temperature was continuously monitored and maintained at 37 $\pm$ 0.5 °C. The mouse's head was fixed in the stereotaxic instrument while the mouse was under deep anesthesia (Anesthesia was induced with 1.25% avertin [0.02 mL/g, i.p.]. When a mouse showed signs of awakening during surgery, an additional dose of 1/2 or 1/3 of the original anesthetic was administered.). The skull was exposed. A saline-dipped cotton swab was used to remove the periosteum, and bregma and lambda were identified. After this, the injection site was aseptically exposed and marked (0.5 mm posterior and 1.0 mm lateral to the bregma, at a depth of 2.5 mm) [21]. The microinjection pump was connected, the air bubbles were expelled, and the needle was inserted vertically and slowly to the target depth. AAV (0.5 µL/min) was delivered to the lateral ventricle using a microsyringe. To ensure optimal delivery, the needle was left in position for 10 min post-injection to prevent backflow. An equivalent volume of AAV-null was administered to the lateral ventricle of the tMCAO/R + NC mice. Upon completion of the infusion, the needle was gradually retracted to avoid pulling on the brain tissue. The skin was sutured. The mouse was placed on a 37 ℃ heating pad until it regained consciousness.

2.3 Drug Administration

LY294002 (S1737, Beyotime Biological Co., Ltd., Shanghai, China) was dissolved in phosphate-buffered saline containing 25% Dimethyl sulfoxide (DMSO, ST038, Beyotime Biological Co., Ltd.) at 50 mM. After dilution, 2 µL of the solution was administered by intracerebroventricular injection to each mouse 1 h before tMCAO induction [22]. LY294002 (a concentration of 10 µM) was supplemented to C8D1A cells (CL-0506, Procell Life Science&Technology Co., Ltd., Wuhan, China) 1 h before oxygen-glucose deprivation/reoxygenation (OGD/R) treatment [23].

2.4 Construction of the tMCAO Model

The middle cerebral artery (MCA) was occluded in an ischemia model using line embolism. To summarize, anesthesia was induced with 1.25% avertin (0.02 mL/g, i.p.). When a mouse showed signs of awakening during surgery,

an additional dose of 1/2 or 1/3 of the original anesthetic was administered. The mouse's vital parameters were continuously tracked to ensure successful completion of the surgery. The procedure involved shaving and sterilizing the neck in preparation for a midline incision that would expose the common carotid artery (CCA), internal carotid artery (ICA), and external carotid artery (ECA). Using surgical thread, the proximal end of the CCA, the distal end of the ICA, and both ends of the ECA were ligated. To occlude the MCA successfully, a tiny incision was made between the ligatures of the ECA. A line embolism then progressed into the ICA through the carotid bifurcation until it reached a mark of approximately 1 cm. After the surgery was completed, the mouse was placed on a heating pad. The line embolism was removed, and the incision was sutured after 1 h of tMCAO. After the mouse regained consciousness, it was placed in an incubator with temperature control for a full day. The only difference in the protocol of the sham group was the absence of MCA occlusion. Reducing the wound size without exposure was the goal of keeping the neck incision small. To ensure the mouse's comfort and rapid recovery, it was kept on a heating pad set at 37 °C from the time it was anesthetized until it regained consciousness [24]. The mice were randomly divided into each experimental group. The sham-operated mice underwent identical surgical exposure without MCA occlusion. The survival rate of the mice reached 90%, and the mice that died or bled were excluded.

2.5 Neurological-Function-Deficit Scoring of the CIRI Model After tMCAO

To evaluate neurological impairments in the mice, the modified Longa score was used. Each mouse underwent neurological function testing, and a researcher who was blind to the aim of the experiment assessed the mice. The scoring system was as follows: 0, no abnormalities; 1, trunk turning to the ipsilateral side when the tail was grasped; 2, the contralateral forelimb showed incomplete extension; 3, turning toward the paralyzed side; 4, leaning toward the opposite side; 5, inability to walk independently, loss of consciousness, or death. If the score was between 1 and 4, the tMCAO model was deemed successful [25]. Mouse data were excluded from the study if (1) the mouse's score was 0 or 5 at the time of euthanasia; (2) the mouse died before euthanasia; or (3) the mouse showed signs of subarachnoid or intraparenchymal hemorrhage.

2.6 2,3,5-Triphenyl Tetrazolium Chloride (TTC) Staining

The mouse was euthanized, and its brain was removed and cut into 6 coronal sections, each 1 mm thick, beginning posterior to the frontal lobe. After 30 min of dark incubation in 2% TTC (G3005, Solarbio, Beijing, China) at 37 °C, the tissue sections were fixed in 4% paraformaldehyde (SI101-01, Sevenbio, Beijing, China). We used ImageJ software (1.53k, National Institutes of Health, Bethesda, MD, USA) to measure the infarct volume after imaging the brain slices. The infarct volume measured by TTC staining was corrected for edema using the formula: corrected infarct volume = volume of the contralateral hemisphere – volume of the viable tissue in the ipsilateral hemisphere. The infarction volume (%) = (contralateral hemisphere volume – ipsilateral hemisphere viable tissue volume)/contralateral hemisphere volume × 100%.

2.7 Brain Water Content (BWC) Detection

The brains were obtained without perfusion, immediately weighed (wet weight). The tissue was dried in an oven for 12 h and re-weighed (dry weight), and the BWC percentage was calculated as: [(wet weight – dry weight)/wet weight] × 100%.

2.8 Immunofluorescence (IF) Staining

The mice's brains were harvested 24 h after tMCAO. After the blood was completely removed by perfusion with 4 °C saline, the mice were perfused with 4% paraformaldehyde until they became stiff. Coronal sections (7 µm thick) prepared using a cryostat (NX50, Thermo Fisher Scientific, Waltham, MA, USA) underwent immunofluorescence staining. After 20 min permeabilization in 0.5% Triton X-100 (BL3087A, Biosharp, Jiangsu, China) at room temperature, sections were blocked with 10% goat serum (AR0009, BOSTER, Wuhan, China) for 1 h. Primary antibodies targeting IL7R (1:100, TD6362, Abmart, Shanghai, China), glial fibrillary acidic protein (GFAP, 1:100, MU184607, Abmart), allograft inflammatory factor 1 (IBA1, 1:1000, MU146067, Abmart), and neuron-specific nuclear protein (NEUN, 1:1000, M050661, Abmart) were applied overnight at 4 °C, followed by 1 h incubation with suitable fluorophore-conjugated secondary antibodies (ZF-0516, ZF-0512 ZSBIO, Beijing, China) at room temperature under light-protected conditions. Nuclear counterstaining was achieved via 4′,6-Diamidino-2-phenylindole (DAPI, BL739A, Biosharp). Fluorescence images were captured using a fluorescence microscopy platform (Nikon Eclipse Ti2, Tokyo, Japan).

2.9 Quantitative Real-Time PCR (RT-qPCR)

RNA isolation was performed using distinct protocols: TRIzol reagent (15596026CN, Invitrogen, Thermo Fisher Scientific) was used for brain tissue samples, and total RNA extraction reagent (BSC51, Biozol, Hangzhou, China) was used for C8D1A cells. After RNA isolation, genomic DNA extraction, and cDNA synthesis were conducted according to the reverse transcription kit (FSQ301, ToYoBo, Tokyo, Japan). The sequences of primers used were as follows: *IL7R-F,* 5′-ACGATTACTTCAAAGGCTTCTGGAG-3′; *IL7R-R,* 5′-AATGGTGACACTTGGCAAGACAG-3′; *Bcl-2-F*, 5′-CTACGAGTGGGATGCTGGAGATG-3′; *Bcl-2-R*, 5′-GGTTGCTCTCAGGCTGGAAGG-3′; *Bax-F*, 5′-GGAGACACCTGAGCTGACCTTG-3′; *Bax-R*, 5′-GCTCCATATTGCTGTCCAGTTCAT-3′; *Caspase3-F*,

5′-GACTGGAAAGCCGAAACTCTTCAT-3′; *Caspase-3-R*, 5′-AGTCCCACTGTCTGTCTCAATG-3′; *β-actin-F*, 5′-GTGCTATGTTGCTCTAGACTTCG-3′; and *β-actin-R*, 5′-ATGCCACAGGATTCCATACC-3′. RT-qPCR analysis was performed on the SLAN-965 system (Hongshi Medical Technology Co., Ltd., Shanghai, China) with SYBR Green Kit reagents (SM143, Sevenbio). Gene expression quantification was performed by the $2^{-\Delta\Delta Ct}$ calculation method.

2.10 Western Blot (WB)

At 24 h after ischemia/reperfusion (I/R) induction, protein samples were obtained from the right hemisphere and C8D1A cells. Protein concentration was quantified using a BCA assay kit (P0010S, Beyotime Biological Co., Ltd.). Electrophoresis was conducted on sodium dodecyl sulfate polyacrylamide gel electrophoresis (SDS-PAGE) gels (12.5% or 10%) loaded with 30 µg of protein per sample. After 1 h of blocking with 5% skim milk at ambient temperature, the membranes were subjected to primary antibodies overnight at 4 °C. The secondary antibodies used were goat anti-rabbit (S0001, 1:3000, Affinity, Jiangsu, China) and goat anti-mouse (1:5000, ZB-2305, ZSBIO) for 1 h. Three Tris Buffered Saline Tween (TBST) washes preceded chemiluminescent detection using the BL520A ECL substrate (Biosharp). The primary antibodies used included IL7R (1:1000, TD6362, Abmart), caspase-3 (1:1000, T40044, Abmart), Bax (1:1000, T40051, Abmart), Bcl-2 (1:1000, T40056, Abmart), PI3K (1:1000, T40115, Abmart), phosphorylated PI3K (1:1000, T40116, Abmart), Akt (1:1000, 4691, Cell Signaling Technology, Danvers, MA, USA), and phosphorylated Akt (1:1000, 4058, Cell Signaling Technology), with GAPDH (1:150,000, 60004-1, Proteintech, Wuhan, China) and β-actin (1:1000, TA-09, ZSBIO) used as loading controls. Band intensity quantification was performed with ImageJ software.

2.11 Cell Culture and Oxygen-Glucose Deprivation/Reoxygenation (OGD/R) Induction

The C8D1A (CL-0506, Procell Life Science & Technology Co., Ltd., Wuhan, China) astrocyte cell line has undergone STR identification and mycoplasma testing, which confirmed that the quality of the C8D1A cell line is correct and there is no mycoplasma contamination. It was cultured in complete medium consisting of Dulbecco's modified Eagle's medium (DMEM, CM-0506, Procell Life Science&Technology Co., Ltd.) supplemented with 10% fetal bovine (CM-0506, Procell Life Science&Technology Co., Ltd.) serum and 1% penicillin/streptomycin [26]. The cell lines were authenticated using DNA short tandem repeat analysis. Cultured cells were placed in a tri-gas incubator with 5% CO_2, 1% O_2, and balanced N_2 for 3 h after being cultured in glucose-free DMEM ($NaHCO_3$, glutamine, sodium pyruvate, serum-free, pH: 7.2–7.4) to induce OGD/R [27]. The cells were then cultivated for 2, 6, 12, 24, or 48 h under normoxic conditions (95% air, 5% CO_2) after restoration of complete medium. The cells that were used as controls were those that were kept under anoxic conditions. This study divided the cells into 5 groups: (1) control; (2) OGD/R; (3) OGD/R + NC; (4) OGD/R + IL7R; and (5) OGD/R + IL7R + LY294002.

2.12 Construction of Stable IL7R-Overexpression Cell Lines by Lentivirus

A lentivirus with a titer of 10^8 TU/mL was generated by cloning the coding sequence of the target gene into the LV5 vector. Gemma Gene Co., Ltd. (Suzhou, Jiangsu, China) generated the lentiviral construct and oversaw its synthesis. To measure the success of transfection, a virus that did not express any GFP was used as a negative control [28]. Once the transfection efficiency surpassed 70%, stable cell line selection was initiated. After lentiviral transfection, stably transfected cells, also known as mixed clones, were selected with puromycin (G04010, Genepharma, Suzhou, China) as a selection factor. The cells were grown and expanded after selection. After that, RNA was taken from the overexpression group and the negative control group for RT-qPCR.

2.13 Cell Counting Kit-8 (CCK-8) Assay

C8D1A astrocytes (4500 cells/well, 96-well plates) were subjected to transfection and OGD/R [29], then incubated with 10 µL CCK-8 (C0037, Beyotime Biological Co., Ltd.) for 1 h. Cell viability was quantified by absorbance at 450 nm on a microplate reader integrated with an optical density detection system (EPOCH, BioTek, Winnsboro, VT, USA).

2.14 Flow Cytometry (Fc)

The rate of neuronal cell apoptosis was measured using the Fc method. After induction of OGD/R and lentiviral transduction, the C8D1A cells were harvested. The cells were assessed by Fc from an Annexin V-APC/7-AAD Apoptosis Detection Kit (abs50008, Absin Biotechnology Co., Ltd., Shanghai, China) [30].

2.15 Transmission Electron Microscopy (TEM) Observation

The C8D1A cell samples were fixed, embedded, dehydrated, and cut into thin slices (60–70 nm). An imaging TEM microscope (H-7700, Hitachi, Tokyo, Japan) was used to examine and photograph these slices.

2.16 Statistical Analysis

Data analysis was conducted with GraphPad Prism version 8.0 software (GraphPad Software, San Diego, CA, USA), and the experimental results are expressed as the means ± standard deviation (SD). The data in each of the experiments were independently obtained at least three times. When the data were normally distributed and showed

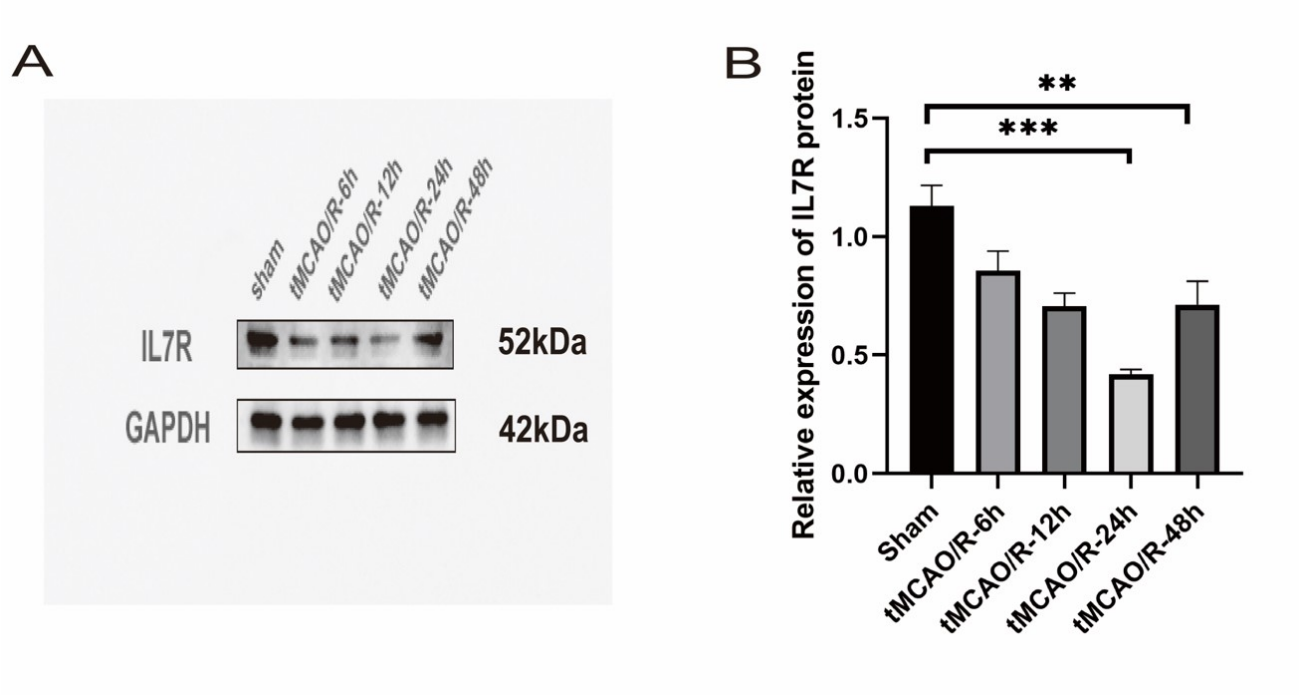

Fig. 1. IL7R protein levels are suppressed at multiple post-tMCAO time points. (A) IL7R protein levels were detected by WB ($n = 7$ per group). (B) The quantitative analysis of IL7R protein in different groups. Data are shown as mean ± SD. The data were analyzed by one-way ANOVA followed by Dunnett posttests. **: $p < 0.01$; ***: $p < 0.001$; IL7R, interleukin-7 receptor; tMCAO, transient middle cerebral artery occlusion; SD, standard deviation; ANOVA, one-way analysis of variance; tMCAO/R, transient middle cerebral artery occlusion/reperfusion.

equal variances, one-way analysis of variance (ANOVA) was performed; otherwise, the Kruskal-Wallis test was performed, with subsequent application of either Dunnett's or Tukey's post hoc tests for multiple comparisons. Statistical significance was considered to be $p < 0.05$. The following thresholds were established for significance markers: *$p < 0.05$; **$p < 0.01$; ***$p < 0.001$, with ns indicating non-significant differences.

3. Results

3.1 Downregulation of IL7R Expression and the Time Course of IL7R in the Mouse Brain After tMCAO

To explore the involvement of IL7R in CIRI, we conducted temporal expression profiling of this receptor in the right cerebral hemisphere after tMCAO. Compared with controls, IL7R expression was significantly downregulated following I/R injury. WB analysis revealed a time-dependent reduction in the IL7R protein level, with the lowest expression observed at 24 h postinjury (Fig. 1A). A marked reduction in IL7R expression was detected at 24 h post-tMCAO ($p < 0.001$), with expression levels starting to recover at 48 h (Fig. 1B, $p < 0.01$). On the basis of these findings, subsequent experiments were conducted 24 h after CIRI induction. These results suggested that IL7R plays a certain role in CIRI.

3.2 IL7R Was Detected in Mouse Brain Astrocytes but not in Neurons or Microglia

In normal brain tissue supplied by the middle cerebral artery of the mice, we performed double IF staining of IL7R with specific markers for astrocytes (GFAP), microglia (IBA1), and neurons (NEUN) (Fig. 2A). IL7R was colocalized with astrocytes, and IL7R was expressed in astrocytes. IL7R was hardly expressed in microglia (Fig. 2B). IL7R was rarely expressed in neurons (Fig. 2C). The Pearson correlation coefficients for these three groups of data were calculated with ImageJ software (Fig. 2D); $|r| > 0.5$ was taken to indicate a clear association (closer to 1 = stronger, closer to 0 = weaker). The Pearson correlation coefficient of the GFAP group was the highest, leading to the conclusion that IL7R is abundantly expressed in astrocytes but rarely expressed in microglia and neurons. In summary, IL7R is detected in astrocytes rather than in neurons or microglia in the mouse brain.

3.3 Verification of Successful Overexpression of IL7R in tMCAO/R Mouse Brain Tissue

AAV-IL7R was injected into the lateral ventricle of mice to induce IL7R overexpression. In mouse brain sections of the MCA supply area treated with AAV-GFP (AAV-ZsGreen, 1.3×10^{12} vector genome/mL), green fluorescence was detected by microscopy, confirming the success of AAV-mediated transduction. We found that GFP green

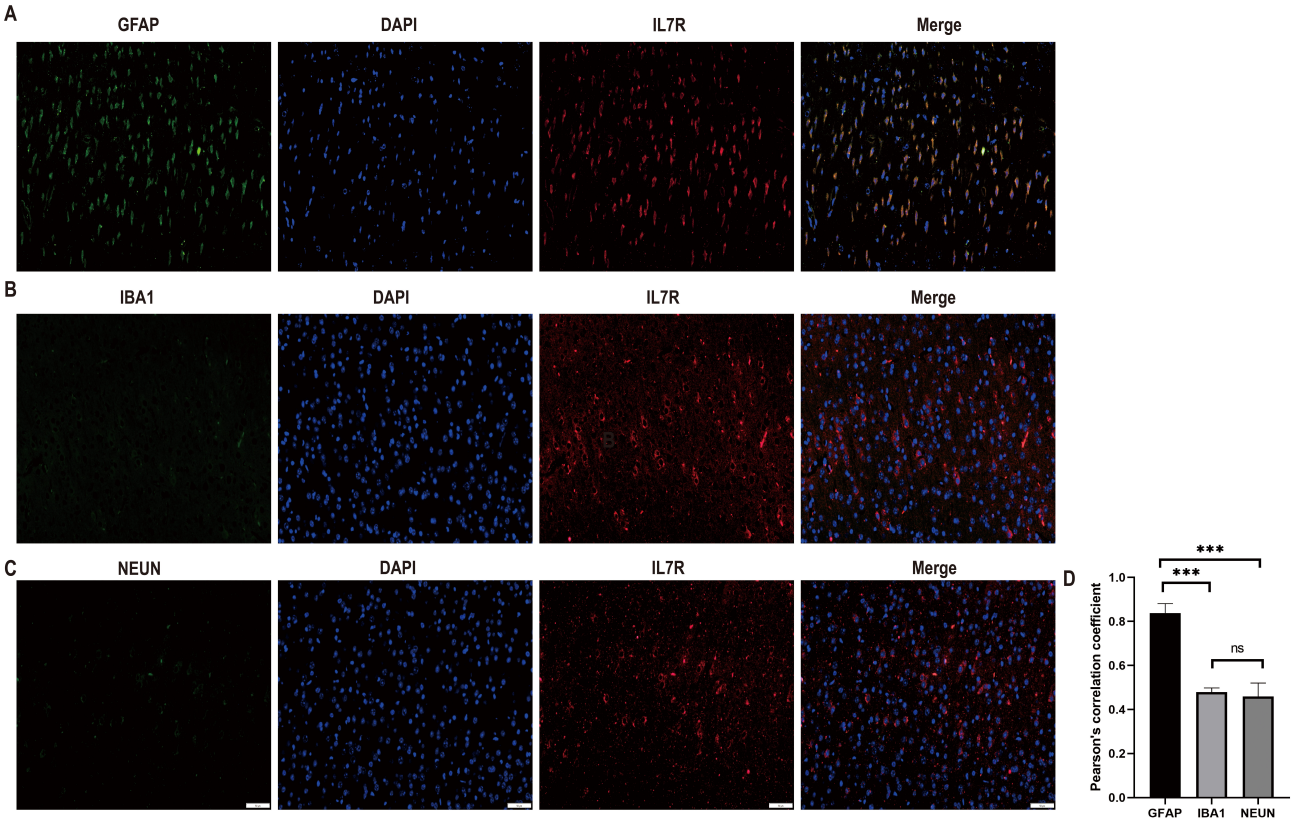

Fig. 2. IF double–staining of IL7R, GFAP, IBA1, and NEUN in mouse brain tissue. (A) Representative images of double-IF staining showing the colocalization of IL7R (red)/GFAP (green)/DAPI (blue). (B) Representative images of double-IF staining showing the colocalization of IL7R (red)/IBA1 (green)/DAPI (blue). (C) Representative images of double-IF staining showing the colocalization of IL7R (red)/NEUN (green)/DAPI (blue). (Scale bar = 50 μm for Fig. 2A–C). (D) The Pearson correlation coefficients for these three groups ($n = 3$ per group). Data are shown as mean ± SD. Data were analyzed by one-way ANOVA followed by Tukey's post hoc test. ns: not significant; ***: $p < 0.001$. IF, Immunofluorescence; GFAP, glial fibrillary acidic protein; DAPI, 4′,6-Diamidino-2-phenylindole; IBA1, allograft inflammatory factor 1; NEUN, neuron-specific nuclear protein.

fluorescence was widely expressed in the brain tissue surrounding the lateral ventricle of the mice (Fig. 3A). Subsequently, colocalization of IL7R with GFAP was assessed by IF double staining. The experimental data indicated that the levels of IL7R and GFAP in the brain tissue of the mice subjected to tMCAO were significantly reduced (Fig. 3C, $p < 0.05$). Comparable levels were maintained between the tMCAO and tMCAO + NC groups. Notably, the experimental group with IL7R overexpression demonstrated substantial increases in both IL7R and GFAP expression in the brain specimens (Fig. 3C, $p < 0.05$). These findings confirmed the localization of IL7R in astrocytes. After tMCAO/R, the level of IL7R decreased, and IL7R was successfully overexpressed. We reached the same conclusion in the RT-qPCR data, and the results confirmed that *IL7R* was successfully overexpressed after pretreatment with AAV-IL7R (Fig. 3D, $p < 0.001$). Furthermore, immunofluorescence triple staining was conducted to verify that IL7R was expressed on the membrane of astrocytes after overexpression of IL7R (**Supplementary Fig. 1**).

3.4 Overexpression of IL7R Reduced CIRI in Mice After tMCAO

In our previous studies, we observed minimal IL7R expression at 24 h post-tMCAO (Fig. 1A), which prompted us to harvest brain tissues at this time point. To determine whether IL7R overexpression mitigates CIRI, we conducted TTC staining (Fig. 4A). Mice treated with IL7R-AAV presented smaller cerebral infarction volumes (Fig. 4A,B, $p < 0.001$). Neurological deficit scores were also assessed, and the results are shown in Fig. 4C. The IL7R-treated group presented lower neurological function scores (Fig. 4C, $p < 0.01$). Additionally, we measured BWC to evaluate cerebral edema induced by tMCAO. BWC was elevated in the tMCAO group (Fig. 4D, $p < 0.001$). However, in the mice treated with IL7R, the BWC was reduced ($p < 0.01$).

3.5 Overexpression of IL7R Reduced Apoptosis After tMCAO

Apoptosis is a critical process in CIRI. Therefore, we investigated the effects of IL7R on apoptosis. The RT-

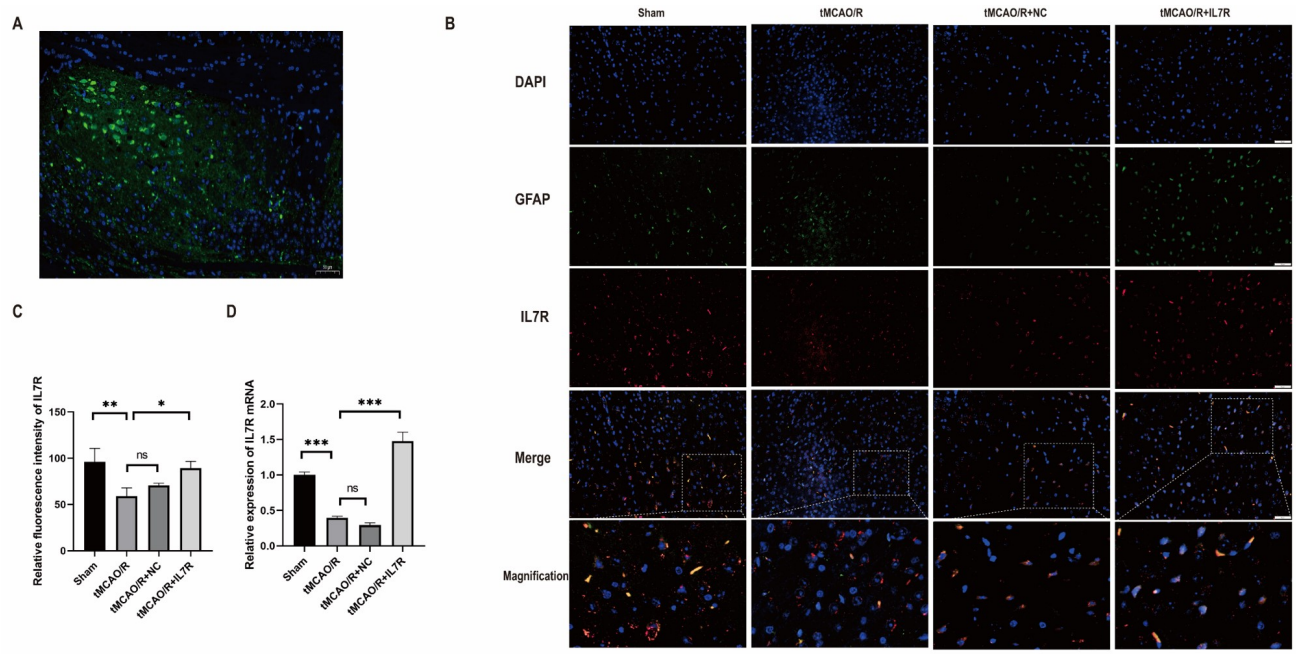

Fig. 3. Verification of successful overexpression of IL7R in tMCAO/R mouse brain tissue. (A) Representative IF image of AAV-GFP-transfected brain sections from mice. (Scale bar = 50 μm). (B) Representative images of double-IF staining showing the colocalization of IL7R (red)/GFAP (green)/DAPI (blue). (Scale bar = 50 μm). (C) Statistical results of IF staining for IL7R in the groups ($n = 3$ per group). (D) Relative mRNA levels of *IL7R* in the sham, tMCAO/R, tMCAO/R + NC, and tMCAO/R + IL7R groups ($n = 3$ per group). Data are shown as mean ± SD from at least three independent experiments. Data were analyzed by one-way ANOVA followed by Tukey's post hoc test. ns: not significant; *: $p < 0.05$; **: $p < 0.01$; ***: $p < 0.001$. AAV, Adeno-Associated Virus; NC, negative control; GFP, Green Fluorescent Protein.

qPCR data revealed substantial elevation in the mRNA levels of *caspase-3* (Fig. 5C, $p < 0.001$) and *Bax* (Fig. 5B, $p < 0.01$), whereas *Bcl-2* mRNA expression was reduced in tMCAO/R mice (Fig. 5A, $p < 0.001$). IL7R treatment reduced *caspase-3* (Fig. 5C, $p < 0.001$) and *Bax* (Fig. 5B, $p < 0.01$) mRNA levels and increased *Bcl-2* mRNA levels (Fig. 5A, $p < 0.001$) after tMCAO/R. WB results confirmed these findings. The overexpression of IL7R elevated the protein level of Bcl-2 (Fig. 5D,E, $p < 0.001$) and decreased the protein expression of Bax (Fig. 5F,G, $p < 0.01$) and caspase-3 (Fig. 5H,I, $p < 0.01$). These effects were reversed by the LY294002 (Fig. 5D–I). Additionally, LY294002 treatment worsened neurological deficits (Fig. 5J, $p < 0.01$) and exacerbated brain edema (Fig. 5K, $p < 0.05$). Together, these results suggested that IL7R reduced CIRI by activating the PI3K/Akt pathway to partially regulate apoptosis.

3.6 Construction of the OGD/R Model and the IL7R Overexpression Model in Mouse Astrocytes

IF staining for IL7R and GFAP in brain tissue revealed that IL7R and GFAP expression were reduced after tMCAO, whereas GFAP expression was increased upon IL7R overexpression. These results confirmed that IL7R was colocalized with astrocytes (Fig. 3B), leading us to select the C8D1A cell line for further *in vitro* validation. Cell viability was assessed *in vitro* at various time points during OGD. Cell viability significantly decreased as the duration of OGD increased. To achieve a cell survival rate of approximately 50%, OGD was set to 3 h (Fig. 6A). In the OGD/R model, *IL7R* mRNA levels were markedly down-regulated by RT-qPCR, particularly after 24 h of OGD/R (Fig. 6B, $p < 0.001$). We applied 3 h of OGD and 24 h of reperfusion to simulate the OGD/R model in C8D1A cells. IL7R overexpression was successfully established in stable transformants. This was indicated by the green fluorescence signal, seen under a fluorescence microscope, in C8D1A cells transfected with lentivirus-green fluorescent protein (LV-GFP) (Fig. 6C). The RT-qPCR analysis confirmed the successful establishment of the *IL7R* overexpression model (Fig. 6D, $p < 0.001$).

3.7 Overexpression of IL7R Reduced Apoptosis After OGD/R In Vitro

Fc assessment was employed to determine the relationship between IL7R and apoptosis *in vitro*. The results revealed that C8D1A cells exposed to OGD/R exhibited a pronounced elevation in apoptotic rate, indicating substantial cellular damage. However, IL7R overexpression significantly reduced apoptosis (Fig. 7A,B; $p < 0.001$). Furthermore, OGD/R markedly reduced cell viability relative to control conditions, but it was notably improved after IL7R overexpression (Fig. 7C, $p < 0.001$). TEM analysis

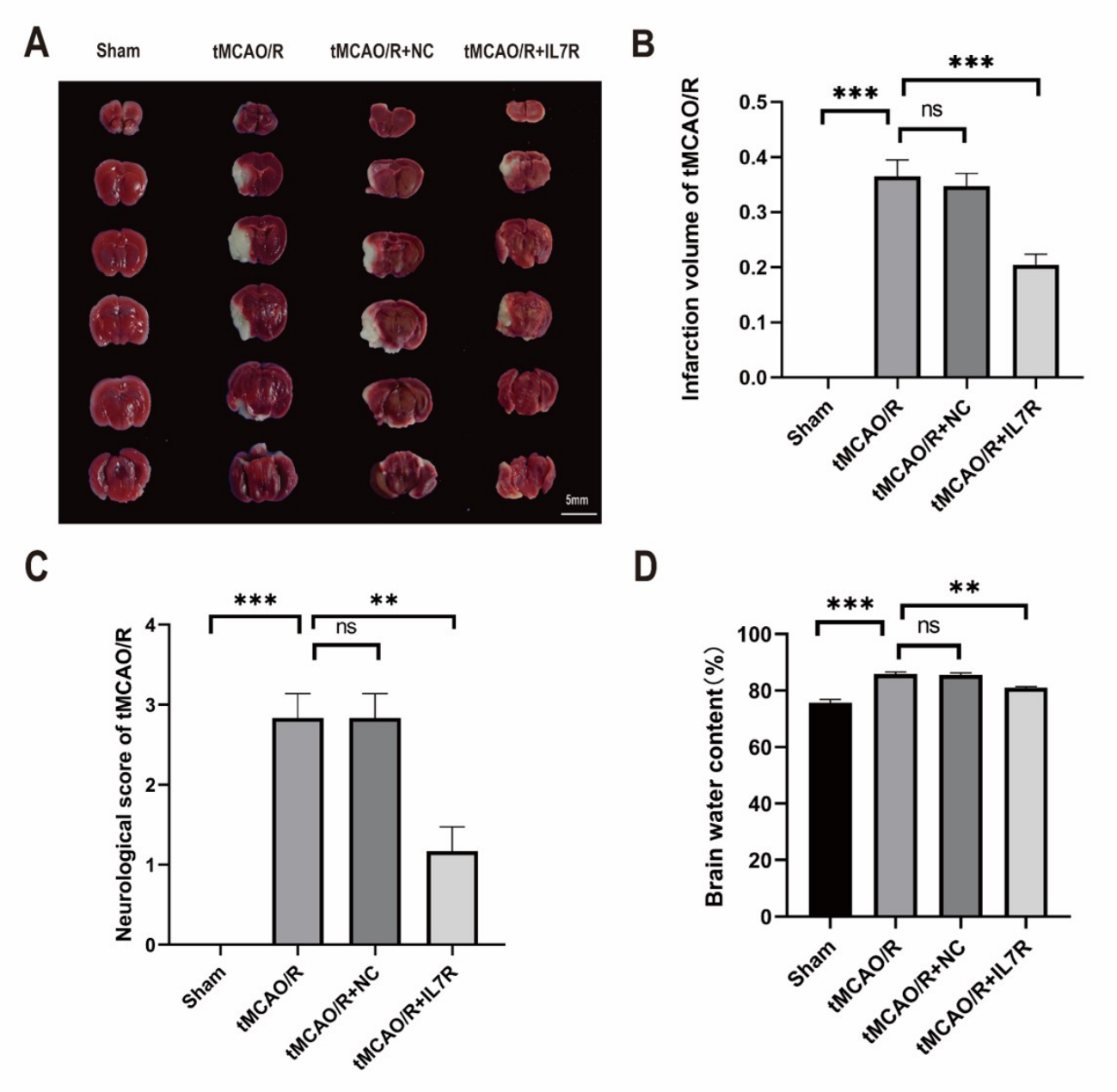

Fig. 4. Overexpression of IL7R enhanced cerebral protection by reducing infarct volume, BWC, and neurological deficit scores *in vivo*. (A) TTC staining of brain tissues after tMCAO/R. (Scale bar = 5 mm). (B) Statistical analysis of the TTC staining results (n = 6 per group). (C) Neurological deficit scores of the mice post-tMCAO/R (n = 6 per group). (D) BWCs in the cerebral hemisphere were measured using the wet and dry weight method (n = 6 per group). Data are shown as mean ± SD. Data were analyzed by one-way ANOVA followed by Tukey's post hoc test. ns: not significant; **: $p < 0.01$; ***: $p < 0.001$. TTC, 2,3,5-Triphenyl Tetrazolium Chloride; BWC, brain water content.

revealed various morphological alterations, such as DNA fragmentation and early apoptotic body formation, in the OGD/R and OGD/R + NC groups. These morphological changes were significantly less in the OGD/R + IL7R group (Fig. 7D). Collectively, these results suggested that IL7R exerts protective effects by inhibiting apoptosis in an *in vitro* model of CIRI.

3.8 IL7R may Regulate Apoptosis via PI3K/Akt-Axis Activation

To investigate the mechanism of IL7R-mediated neuroprotection via PI3K/Akt signaling in CIRI, pharmacological inhibition was implemented using LY294002, preceding IL7R overexpression and OGD/R induction. The RT-qPCR data revealed a marked reduction in *Bcl-2*, in parallel with elevated *Bax* and *caspase-3* expression, in the

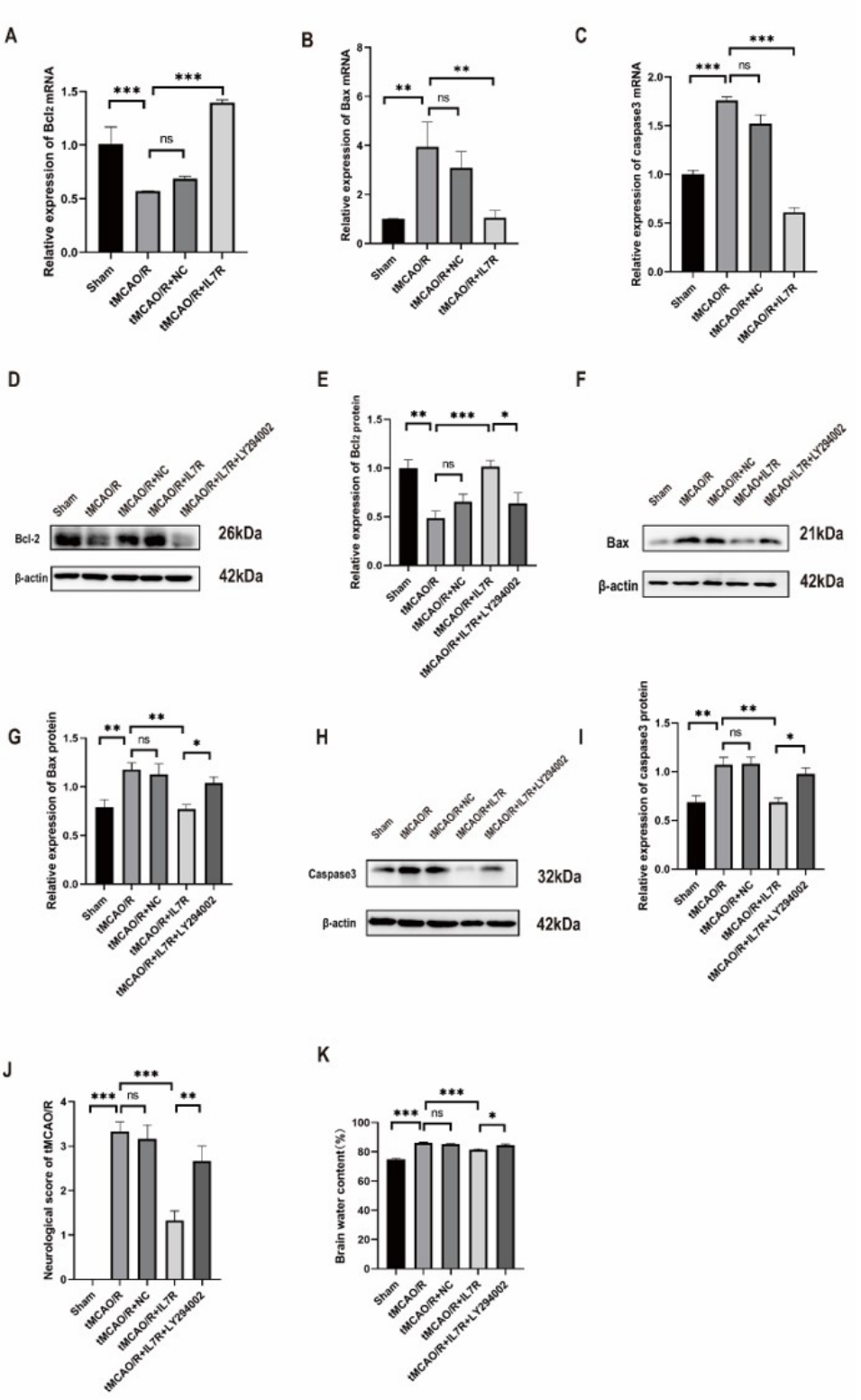

Fig. 5. The overexpression of IL7R improved the cerebral-protective effects by reducing apoptosis after tMCAO *in vivo*. (A–C) Relative mRNA levels of (A) *Bcl-2*, (B) *Bax*, and (C) *caspase-3* in the sham, tMCAO/R, tMCAO/R + NC, and tMCAO/R + IL7R groups ($n = 3$ per group). (D–I) WB and quantitative analysis of Bcl-2, Bax, and caspase-3 protein levels in the sham, tMCAO/R, tMCAO/R + NC, tMCAO/R + IL7R, and tMCAO/R + IL7R + LY294002 groups ($n = 7$ per group). (J) Neurological deficit scores of each group of mice ($n = 6$ per group). (K) BWC of each group of mice ($n = 6$ per group). Data are shown as mean ± SD from at least three independent experiments. Data were analyzed by one-way ANOVA followed by Tukey's post hoc test. ns: not significant; *: $p < 0.05$; **: $p < 0.01$; ***: $p < 0.001$. WB, western blot; Bcl-2, B-cell lymphoma 2; Bax, Bcl-2-associated X protein; LY294002, PI3K pathway inhibitor.

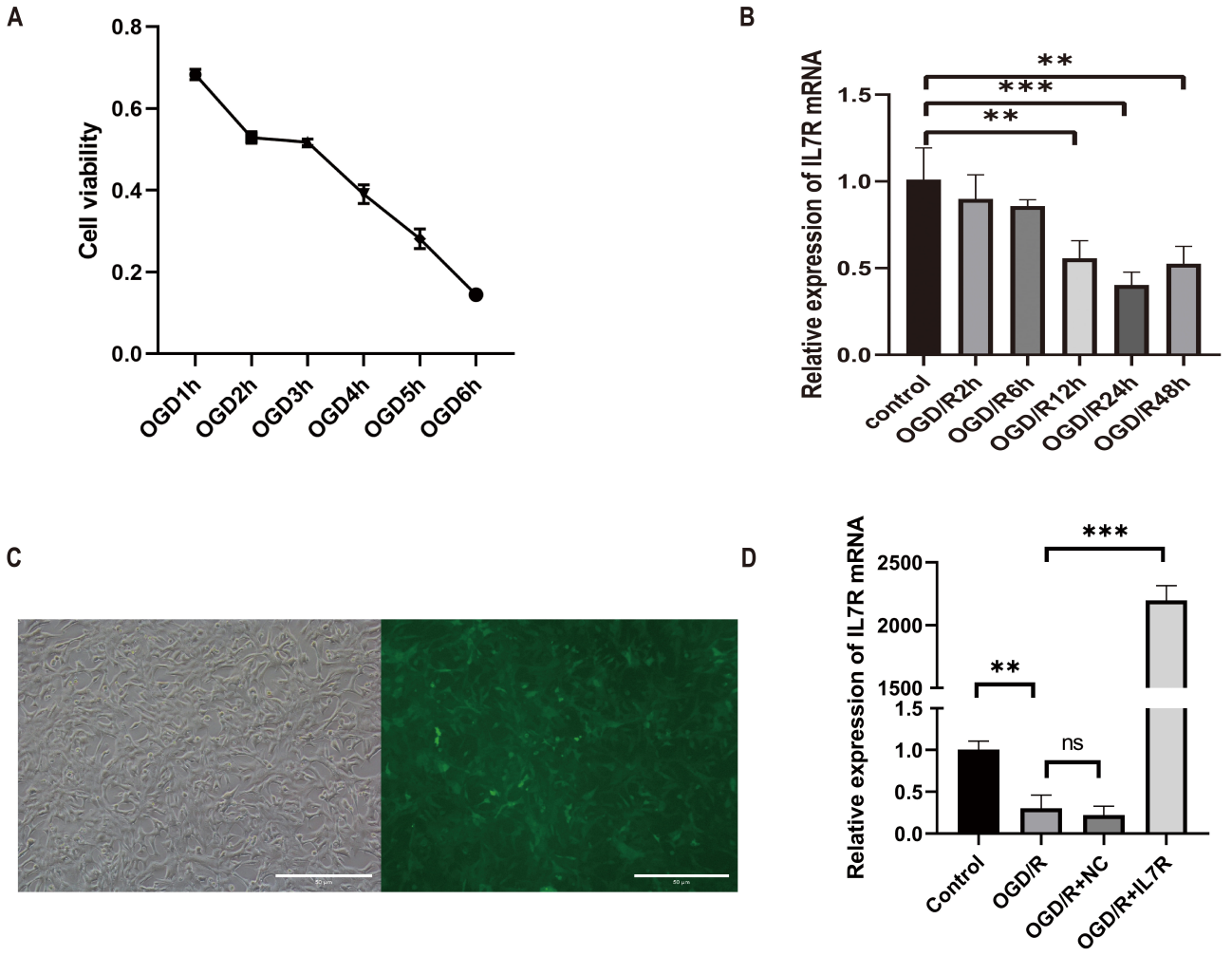

Fig. 6. Generation of an OGD/R model and an IL7R overexpression model in mouse brain astrocytes. (A) Cell viability analysis via CCK-8 assays after various durations of OGD (1, 2, 3, 4, 5, or 6 h), followed by 24 h of reoxygenation ($n = 3$ per group). (B) *IL7R* expression was significantly downregulated in OGD/R-exposed C8D1A cells. RT-qPCR analysis confirmed the significant decreasing in *IL7R* mRNA levels at 24 h of OGD/R ($n = 3$ per group). (C) Representative IF images of LV-IL7R and GFP-transfected C8D1A cells under normal and fluorescence microscopy. (Scale bar = 50 μm). (D) Relative mRNA levels and quantitative analysis of *IL7R* ($n = 3$ per group). Data are shown as mean ± SD from at least three independent experiments. The data of B were analyzed by one-way ANOVA followed by Dunnett posttests, and the rest of the data were analyzed by one-way ANOVA followed by Tukey's post hoc test. ns: not significant; **: $p < 0.01$; ***: $p < 0.001$. OGD/R, oxygen-glucose deprivation/reoxygenation; CCK-8, Cell Counting Kit-8; LV-IL7R, lentivirus-IL7R.

OGD/R model. The overexpression of *IL7R* counteracted these alterations, resulting in significant enhancement of the *Bcl-2* mRNA level and concurrent suppression of the *Bax* and *caspase-3* mRNAs. Conversely, pharmacological PI3K inhibition with LY294002 abolished the antiapoptotic effects mediated by *IL7R* overexpression (Fig. 8A–C, $p < 0.05$), indicating the involvement of the PI3K/Akt pathway. Subsequent WB analysis corroborated these observations, revealing increased Bcl-2, phosphorylated PI3K (p-PI3K), and activated Akt (p-Akt) protein expression coupled with decreased Bax and caspase-3 levels post–OGD/R treatment in the IL7R-overexpressing groups (Fig. 8D–M). Additionally, LY294002 reversed the protective effects of IL7R overexpression, as indicated by reduced cell viability (Fig. 8N) and decreased levels of Bcl-2 (Fig. 8D,E), p-PI3K (Fig. 8J,K), and p-Akt (Fig. 8L,M) but increased Bax (Fig. 8F,G) and caspase-3 (Fig. 8H,I) protein levels (all $p < 0.05$). Together, the data pinpoint PI3K/Akt signaling as the operative route through which IL7R suppresses apoptosis.

4. Discussion

Our results observed that IL7R level was downregulated in the cerebral I/R model. Furthermore, IL7R overexpression protected against CIRI. Our results demonstrated that IL7R overexpression reduced cerebral edema, conferred better neurological outcome, and limited both in-

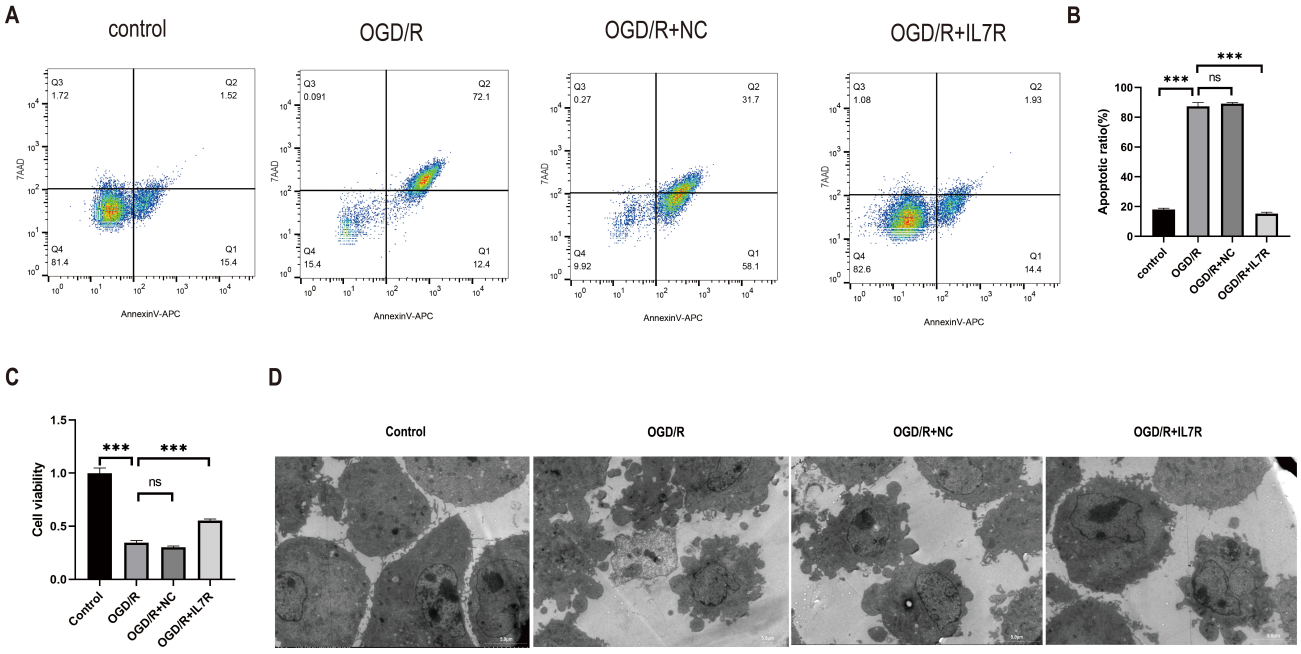

Fig. 7. IL7R overexpression reduced apoptosis after OGD/R *in vitro*. (A,B) Fc and quantitative analysis of apoptosis rates in C8D1A cells across different groups (n = 3 per group). (C) Cell viability analysis with the CCK-8 assay (n = 3 per group). (D) Representative TEM images of C8D1A cells (Scale bar = 5.0 μm). Data are shown as mean ± SD from at least three independent experiments. Data were analyzed by one-way ANOVA followed by Tukey's post hoc test. ns: not significant; ***: $p < 0.001$. Fc, Flow Cytometry; TEM, Transmission Electron Microscopy.

farct expansion and apoptosis after I/R. The overexpression of IL7R led to decreased Bax and caspase-3 expression and elevated Bcl-2 levels. LY294002 largely reversed IL7R-mediated protection against CIRI, confirming that PI3K/Akt signaling partially drives the beneficial effect (Fig. 9).

Globally, IS ranks among the foremost causes of long-term disability and death. Vascular recanalization therapy has become widely applied clinically, with early reperfusion considered to be the most effective treatment for IS [31]. However, reperfusion itself can trigger additional pathological mechanisms that worsen brain damage [32]. IL-7 is a crucial homeostatic cytokine that supports the persistence and viability of T-cell and other lymphoid populations [33]. IL-7 is associated with inflammation, autoimmune conditions, neoplastic diseases, and various biological processes [34]. IL-7 transcripts are detectable in both lymphoid and non-lymphoid tissues, which are essential for biological barriers [35]. IL7R is likewise indispensable for the ontogeny and continued survival of multiple immune-cell lineages and is involved in diseases linked to lymphatic dysfunction [36]. Furthermore, IL7R is involved in neurodegenerative-disease pathology, including Parkinson's disease and multiple sclerosis [37,38]. The IL-7/IL7R signaling pathway influences inflammation after intracerebral hemorrhage and may be a new immunotherapy target in the pathophysiological mechanism of intracerebral hemorrhage treatment [39]. The reduced expression of IL7R has been correlated with delayed myelination [40]. IL-7 also has trophic properties in the developing brain, suggesting its potential as a growth factor for neurons of physiological value [41]. These observations suggest a potential neuroprotective function for IL7R. The result of a porcine femoral artery I/R study indicated that dynamic changes occurred in gene expression after I/R. These changes may be closely related to T-cell activation. During T-cell activation, increased IL7R potentially orchestrates I/R injury [42]. In the myocardial I/R model, IL-7 intensified cardiac injury by modulating macrophage infiltration and polarization. Controlling the level of IL-7 may help alleviate myocardial I/R injury [43]. However, the role of IL7R in CIRI has yet to be explored. We found that IL7R expression was downregulated after IS and inversely correlated with infarct size and neurological deficits, indicating that IL7R may be a critical player in CIRI and a potential therapeutic target. However, the exact molecular basis of IL7R action requires further exploration.

Previous studies have shown that certain protein-coding genes orchestrate apoptosis control; whether *IL7R* participates in a regulatory network with these genes remains to be explored. Future research can explore the specific mechanisms of these proteins in different disease states. Silent Information Regulator1 (SIRT1) suppresses apoptotic signaling, curbs neuro-inflammation by reducing pro-inflammatory cytokine release, and preserves mitochondrial integrity, thereby conferring broad neuroprotec-

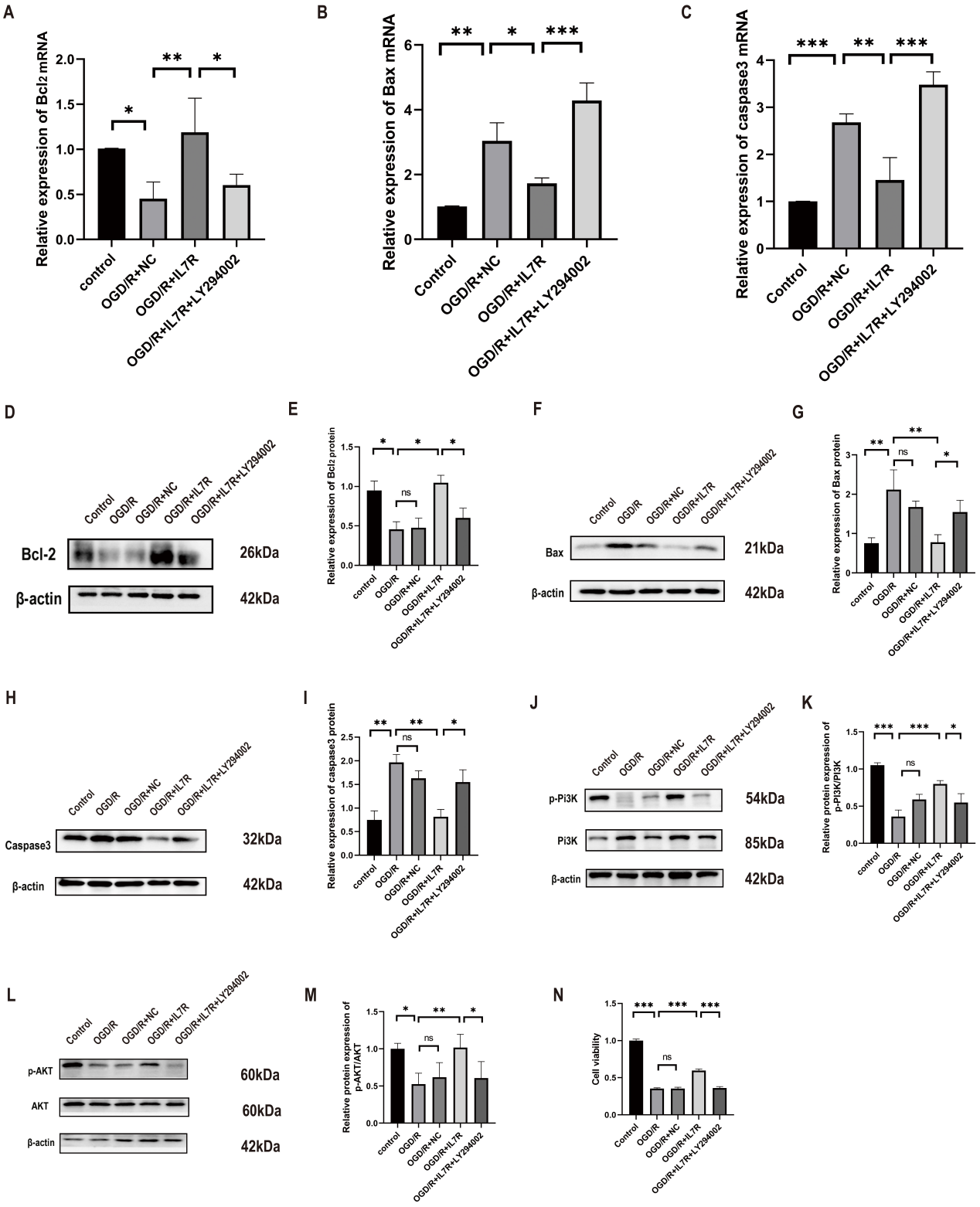

Fig. 8. LY294002 reversed the ability of IL7R to inhibit apoptosis after CIRI. (A–C) Relative mRNA levels and quantitative analysis of *Bcl-2*, *Bax*, and *caspase-3* ($n = 3$ per group). (D–M) Representative WB images and quantitative analysis of Bcl-2 (D,E), Bax (F,G), caspase-3 (H,I), p-PI3K/PI3K (J,K), and p-Akt/Akt (L,M) protein levels in C8D1A cells of different groups ($n = 3$ per group). (N) Cell viability of C8D1A cells in different groups ($n = 5$ per group). Data are shown as mean ± SD from at least three independent experiments. Data were analyzed by one-way ANOVA followed by Tukey's post hoc test. ns: not significant; *: $p < 0.05$; **: $p < 0.01$; ***: $p < 0.001$. CIRI, Cerebral ischemia-reperfusion injury; p-PI3K, phosphorylated phosphatidylinositol 3-kinase; PI3K, phosphatidylinositol 3-kinase; p-Akt, phosphorylated protein kinase B; Akt, protein kinase B.

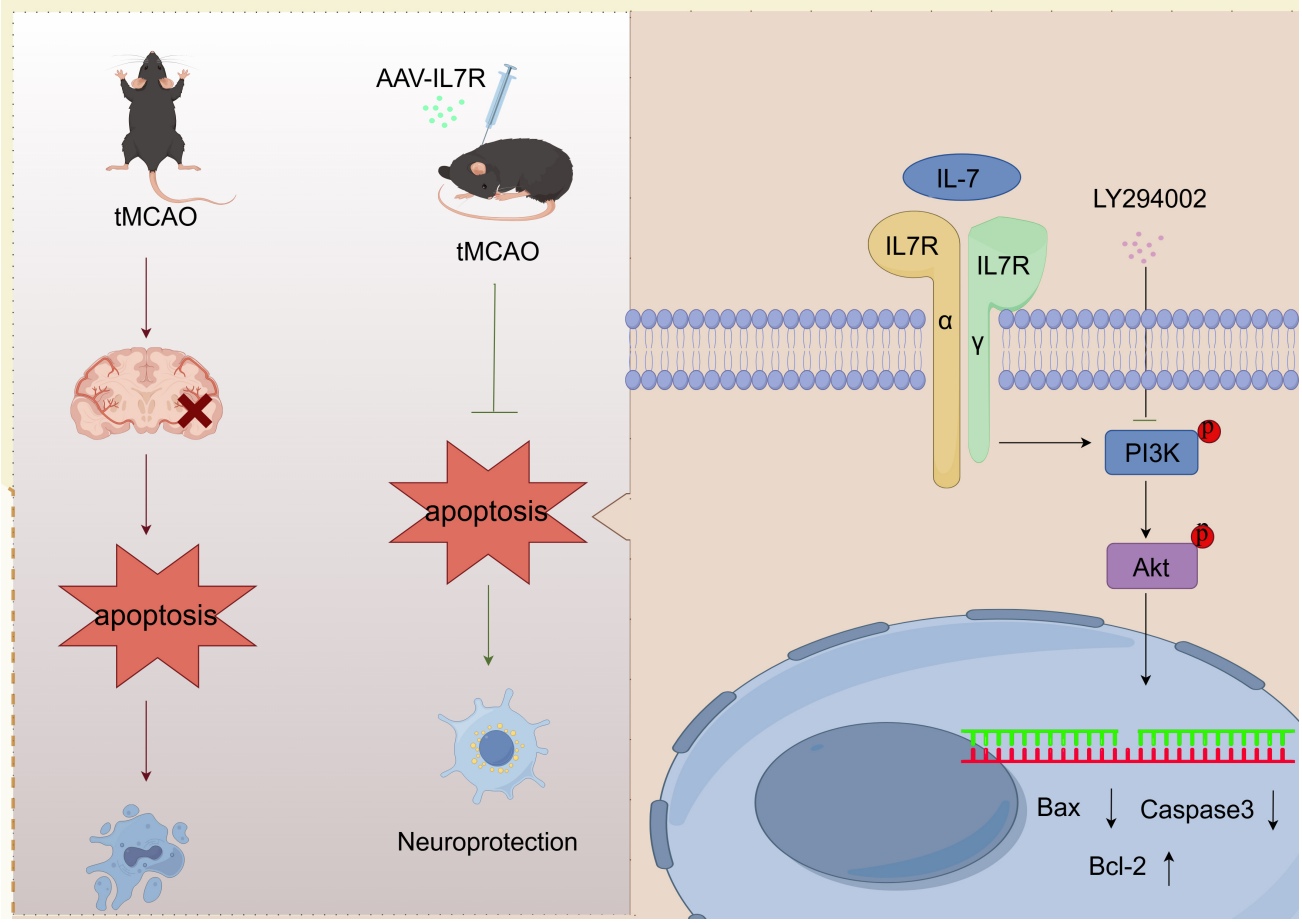

Fig. 9. The mechanism by which IL7R may attenuate astrocyte apoptosis through PI3K/Akt pathway activation after cerebral I/R. Figdraw provided the material for drawing (https://www.figdraw.com/). I/R, ischemia/reperfusion.

tion against CIRI [44–46]. These pleiotropic effects make SIRT1 a promising therapeutic target in stroke. Emerging evidence has suggested that SIRT1 may also govern IL7R expression. In NSCLC, SIRT1 modulated IL7R levels on immune cells, shaping tumor prognosis [47], and loss of SIRT1 paralleled down-regulated IL7R and subsequent T-cell dysfunction in COVID-19 [48]. Although a direct SIRT1–IL7R axis has not yet been validated in CIRI, their complementary cytoprotective and immunomodulatory roles imply that an interaction could influence ischemic outcome. Future studies should therefore determine whether SIRT1 regulates IL7R after stroke and whether co-targeting both molecules might augment recovery. Furthermore, small extracellular vesicles derived from mesenchymal stromal cells have recently been shown to markedly enhance neural recovery and brain remodeling in both young and aged rats after permanent distal MCAO [49], underscoring their therapeutic promise for elderly stroke patients. Estrogen additionally confers cerebrovascular protection, emphasizing that advanced age and female sex are critical determinants of CIRI severity and outcome. However, our present work did not stratify animals by age or sex, a limitation that will be addressed in follow-up studies designed to dissect how these variables modulate CIRI pathobiology and to translate the findings into sex- and age-tailored strategies for human stroke prevention and rehabilitation.

The pathogenesis of IS is multifaceted and involves disturbances in energy metabolism, inflammatory responses, and apoptosis [50,51]. Inflammation and apoptosis induced by the activation of astrocytes are central pathological mechanisms in CIRI. The neuroprotective effects observed during CIRI are due to the inhibition of astrocyte apoptosis [52]. The study has revealed that CIRI has protective effects against neuronal damage via the inhibition of apoptosis [14]. Apoptosis constitutes the main driver of neuronal death after ischemia. Therefore, attenuating apoptosis is essential for improving the outcome of CIRI [53]. IL7R has been shown to regulate apoptosis in other diseases. Liu and colleagues [18] demonstrated that IL-7/IL7R signaling suppresses apoptosis in NSCLC cells by modulating Bcl-2 and Bax through the p53 pathway. IL7R also triggers the Janus kinase1 (JAK1)/STAT5 pathway to increase Bcl-2 expression in pancreatic-duct adenocarcinoma [54], as IL7R has been implicated in demyelination and the process of oligodendrocyte apoptosis [37]. These results collectively emphasize the antiapoptotic ef-

fects of IL7R in various diseases. However, the specific relationship between IL7R and apoptosis in CIRI had not previously been explored. Therefore, we actively investigated whether IL7R functions in regulating apoptosis in CIRI. Our study explored whether IL7R regulated apoptosis in CIRI; results revealed that IL7R does protect against apoptosis in CIRI. Specifically, the overexpression of IL7R resulted in a decreased infarct volume and enhanced neurological outcomes (Fig. 4), decreased level of proapoptotic proteins, and a reduced rate of apoptosis while increasing the level of the antiapoptotic protein (Fig. 5). We found that IL7R can mediate neuroprotection by exerting antiapoptotic effects, which aligns with earlier reports. Our findings confirmed that IL7R protects against CIRI through antiapoptotic mechanisms and provide a foundation for the development of IL7R-based therapies for ischemic brain diseases.

The PI3K/Akt signaling cascade is central to the pathobiology of CIRI and has well-documented neuroprotective characteristics [55]. Catalpol administration enhanced the neurovascular unit in an IS model by activating the PI3K/Akt [56]. Colin has antiapoptotic effects on cardiomyocytes by regulating the PI3K/Akt [57]. Resveratrol administration alleviated apoptosis in stroke models through the PI3K/Akt pathway [58]. IL7R affects hematopoiesis and immune responses through the JAK-STAT and PI3K/Akt pathways [12]. IL-7 activates the autophagy process in lung cancer cells through the PI3K/Akt [17]. Our data revealed that IL7R, through the PI3K/Akt pathway, is involved in the modulation of apoptosis. To substantiate the pathway-specific neuroprotection hypothesis, we used pharmacological PI3K inhibition with LY294002 and effectively attenuated the IL7R-mediated protective effects (Fig. 5). Although gene knockout or co-immunoprecipitation methods can increase the specificity of the pathway, LY294002 has been widely recognized for this application [59]. These cumulative results establish PI3K/Akt signaling as an essential mediator of the therapeutic potential of IL7R in CIRI management; however, whether the mitogen-activated protein kinase (MAPK), JAK-STAT, and other specific regulatory mechanisms are involved in this process requires further exploration in the future.

Our study had several limitations. First, the animal sample in some experiments was not large, which was a decision made to minimize animal use, according to NIH recommendations. Although this approach enhanced the ethical standard of the research, it limited the statistical power for detecting more subtle effects. Second, for the experiments involving the PI3K inhibitor LY294002, a separate vehicle-control group was not included. Instead, comparisons were made against the standard model control group. Although the effects of the solvent DMSO were expected to be minimal based on common practice and previous literature, the absence of a dedicated control group meant that we could not entirely rule out its potential contribution to the observed effects. It is noteworthy that the assessment of neurological function in this study was conducted using the modified Longa score, a well-validated tool for global deficit evaluation. Future studies incorporating more specialized tests for motor coordination, balance, and strength will be valuable in order to delineate the specific facets of functional recovery influenced by IL7R overexpression. In addition, the precise contribution of the IL-7 ligand remains undefined; the upstream and the downstream regulatory networks controlled by IL7R require further exploration. Consequently, clinical translation of IL7R-based interventions will demand extensive additional investigation.

Overall, this study provided new insights and potential therapeutic avenues for treating CIRI. Our observations suggested that the overexpression of IL7R diminishes apoptosis levels by modulating the interactions of proteins associated with apoptosis, thereby mitigating CIRI, probably consequent to PI3K/Akt activation. Nevertheless, additional research is essential to elucidate, comprehensively, the precise pathway mechanisms associated with molecules both upstream and downstream of IL7R.

5. Conclusion

Collectively, our experimental data demonstrate that IL7R administration confers neuroprotection against cerebral damage and apoptotic processes through stimulation of the PI3K/Akt. Our results identify IL7R as a candidate target for CIRI therapy. Although its precise molecular actions remain to be fully defined, the approach holds clear translational promise and offers a fresh direction for developing effective CIRI interventions.

Availability of Data and Materials

The data supporting the findings of this study are available from the corresponding author upon reasonable request.

Author Contributions

SY conceived the study, performed the experiments, analyzed the data, drew the graphs, and wrote the manuscript. QS, WL, and DM participated in some animal model experiments. ZS participated in the conception process and guided and revised the manuscript. All authors contributed to editorial changes in the manuscript. All authors read and approved the final manuscript. All authors have participated sufficiently in the work and agreed to be accountable for all aspects of the work.

Ethics Approval and Consent to Participate

Strict adherence to the U.S. National Institutes of Health (NIH) criteria for the care and use of animals was maintained throughout the investigation and the research was approved by the Institutional Animal Ethics Committee of the First Affiliated Hospital of Harbin Medical Univer-

sity (Ethics No. 2023124). Efforts were made to minimize the number of mice used and to alleviate their pain as much as possible. The procedure was strictly followed by the guidelines approved by the Institutional Animal Care and Use Committee, with the guiding principles of minimizing pain, ensuring rapid death, and respecting animal life.

Acknowledgment

We are grateful for the help provided by the teachers and students of the Central Laboratory of the First Affiliated Hospital of Harbin Medical University during the experiment. Figdraw provided the material for drawing (https://www.figdraw.com/).

Funding

This study was supported by the Graduate Research Allowance of the First Affiliated Hospital of Harbin Medical University.

Conflict of Interest

The authors declare no conflict of interest.

Supplementary Material

Supplementary material associated with this article can be found, in the online version, at https://doi.org/10.31083/JIN46638.

References

[1] Kaji R. Global burden of neurological diseases highlights stroke. Nature Reviews. Neurology. 2019; 15: 371–372. https://doi.org/10.1038/s41582-019-0208-y.

[2] Xie Q, Li H, Lu D, Yuan J, Ma R, Li J, *et al*. Neuroprotective Effect for Cerebral Ischemia by Natural Products: A Review. Frontiers in Pharmacology. 2021; 12: 607412. https://doi.org/10.3389/fphar.2021.607412.

[3] Satue E, Vila-Corcoles A, Ochoa-Gondar O, de Diego C, Forcadell MJ, Rodriguez-Blanco T, *et al*. Incidence and risk conditions of ischemic stroke in older adults. Acta Neurologica Scandinavica. 2016; 134: 250–257. https://doi.org/10.1111/ane.12535.

[4] Khanevski AN, Bjerkreim AT, Novotny V, Naess H, Thomassen L, Logallo N, *et al*. Recurrent ischemic stroke: Incidence, predictors, and impact on mortality. Acta Neurologica Scandinavica. 2019; 140: 3–8. https://doi.org/10.1111/ane.13093.

[5] Su JH, Wu GP, Peng X, Zhao GQ, Peng Y, Zhang HH, *et al*. Neuroprotective Effects of an *N*-Salicyloyl Tryptamine Derivative against Cerebral Ischemia/Reperfusion Injury. ACS Chemical Neuroscience. 2023; 14: 2146–2158. https://doi.org/10.1021/acschemneuro.3c00149.

[6] Lu D, Yang Y, Huang G, Ye Q, Quan X, Kaltwasser B, *et al*. MFN2 and BAG6 Synergistically Protect Against Cerebral Reperfusion Injury by Regulating ROS Levels and Autophagic Flux. Stroke. 2025; 56: 3468–3483. https://doi.org/10.1161/STROKEAHA.125.052689.

[7] Nguyen V, Mendelsohn A, Larrick JW. Interleukin-7 and Immunosenescence. Journal of Immunology Research. 2017; 2017: 4807853. https://doi.org/10.1155/2017/4807853.

[8] Lin J, Zhu Z, Xiao H, Wakefield MR, Ding VA, Bai Q, *et al*. The role of IL-7 in Immunity and Cancer. Anticancer Research. 2017; 37: 963–967. https://doi.org/10.21873/anticanres.11405.

[9] Wang C, Kong L, Kim S, Lee S, Oh S, Jo S, *et al*. The Role of IL-7 and IL-7R in Cancer Pathophysiology and Immunotherapy. International Journal of Molecular Sciences. 2022; 23: 10412. https://doi.org/10.3390/ijms231810412.

[10] Guo F, Wang CY, Wang S, Zhang J, Yan YJ, Guan ZY, *et al*. Alteration in gene expression profile of thymomas with or without myasthenia gravis linked with the nuclear factor-kappaB/autoimmune regulator pathway to myasthenia gravis pathogenesis. Thoracic Cancer. 2019; 10: 564–570. https://doi.org/10.1111/1759-7714.12980.

[11] Moore AJ, In TS, Trotman-Grant A, Yoganathan K, Montpellier B, Guidos CJ, *et al*. A key role for IL-7R in the generation of microenvironments required for thymic dendritic cells. Immunology and Cell Biology. 2017; 95: 933–942. https://doi.org/10.1038/icb.2017.74.

[12] Wang Y, Schafer CC, Hough KP, Tousif S, Duncan SR, Kearney JF, *et al*. Myeloid-Derived Suppressor Cells Impair B Cell Responses in Lung Cancer through IL-7 and STAT5. Journal of Immunology (Baltimore, Md.: 1950). 2018; 201: 278–295. https://doi.org/10.4049/jimmunol.1701069.

[13] Park JH, Waickman AT, Reynolds J, Castro M, Molina-París C. IL7 receptor signaling in T cells: A mathematical modeling perspective. Wiley Interdisciplinary Reviews. Systems Biology and Medicine. 2019; 11: e1447. https://doi.org/10.1002/wsbm.1447.

[14] Fan Y, Li Y, Yang Y, Lin K, Lin Q, Luo S, *et al*. Chlorogenic acid promotes angiogenesis and attenuates apoptosis following cerebral ischaemia-reperfusion injury by regulating the PI3K-Akt signalling. Pharmaceutical Biology. 2022; 60: 1646–1655. https://doi.org/10.1080/13880209.2022.2110599.

[15] Storek J, Nash RA, McSweeney PA, Furst DE, Sullivan KM. Normal interleukin-7 (IL7) levels and normal IL7 response to CD4 T lymphopenia in patients with multiple sclerosis and systemic sclerosis. Clinical Immunology (Orlando, Fla.). 2006; 121: 118–119. https://doi.org/10.1016/j.clim.2006.05.016.

[16] Ross C, Sharma M, Paul J, Srivastava S. Microarray analysis reveals distinct immune signatures in *BCR-ABL* positive and negative myeloproliferative neoplasms. Indian Journal of Cancer. 2023; 60: 24–31. https://doi.org/10.4103/ijc.IJC_21_20.

[17] Jian M, Yunjia Z, Zhiying D, Yanduo J, Guocheng J. Interleukin 7 receptor activates PI3K/Akt/mTOR signaling pathway via downregulation of Beclin-1 in lung cancer. Molecular Carcinogenesis. 2019; 58: 358–365. https://doi.org/10.1002/mc.22933.

[18] Liu ZH, Wang MH, Ren HJ, Qu W, Sun LM, Zhang QF, *et al*. Interleukin 7 signaling prevents apoptosis by regulating bcl-2 and bax via the p53 pathway in human non-small cell lung cancer cells. International Journal of Clinical and Experimental Pathology. 2014; 7: 870–881.

[19] Gris T, Laplante P, Thebault P, Cayrol R, Najjar A, Joannette-Pilon B, *et al*. Innate immunity activation in the early brain injury period following subarachnoid hemorrhage. Journal of Neuroinflammation. 2019; 16: 253. https://doi.org/10.1186/s12974-019-1629-7.

[20] Percie du Sert N, Hurst V, Ahluwalia A, Alam S, Avey MT, Baker M, *et al*. The ARRIVE guidelines 2.0: Updated guidelines for reporting animal research. PLoS Biology. 2020; 18: e3000410. https://doi.org/10.1371/journal.pbio.3000410.

[21] Huang Y, Huang W, Huang Y, Song P, Zhang M, Zhang HT, *et al*. Cdk5 Inhibitory Peptide Prevents Loss of Neurons and Alleviates Behavioral Changes in p25 Transgenic Mice. Journal of Alzheimer's Disease: JAD. 2020; 74: 1231–1242. https://doi.org/10.3233/JAD-191098.

[22] Miao J, Wang L, Zhang X, Zhu C, Cui L, Ji H, *et al*. Protective Effect of Aliskiren in Experimental Ischemic Stroke: Up-Regulated p-PI3K, p-AKT, Bcl-2 Expression, Attenuated Bax Expression. Neurochemical Research. 2016; 41: 2300–2310. https://doi.org/10.1007/s11064-016-1944-7.

[23] Wu J, Feng X, Zhang B, Li J, Xu X, Liu J, *et al*. Blocking the bFGF/STAT3 interaction through specific signaling pathways induces apoptosis in glioblastoma cells. Journal of Neuro-oncology. 2014; 120: 33–41. https://doi.org/10.1007/s11060-014-1529-8.

[24] Percie du Sert N, Ahluwalia A, Alam S, Avey MT, Baker M, Browne WJ, *et al*. Reporting animal research: Explanation and elaboration for the ARRIVE guidelines 2.0. PLoS Biology. 2020; 18: e3000411. https://doi.org/10.1371/journal.pbio.3000411.

[25] Wan Y, Huang L, Liu Y, Ji W, Li C, Ge RL. Preconditioning With Intermittent Hypobaric Hypoxia Attenuates Stroke Damage and Modulates Endocytosis in Residual Neurons. Frontiers in Neurology. 2021; 12: 750908. https://doi.org/10.3389/fneur.2021.750908.

[26] Zhang H, Liu S, Qin Q, Xu Z, Qu Y, Wang Y, *et al*. Genetic and Pharmacological Inhibition of Astrocytic Mysm1 Alleviates Depressive-Like Disorders by Promoting ATP Production. Advanced Science (Weinheim, Baden-Wurttemberg, Germany). 2022; 10: e2204463. https://doi.org/10.1002/advs.202204463.

[27] Yang X, Yun Y, Wang P, Zhao J, Sun X. Upregulation of RCAN1.4 by HIF1α alleviates OGD-induced inflammatory response in astrocytes. Annals of Clinical and Translational Neurology. 2022; 9: 1224–1240. https://doi.org/10.1002/acn3.51624.

[28] Jiang XL, Zhang ZB, Feng CX, Lin CJ, Yang H, Tan LL, *et al*. PHLDA1 contributes to hypoxic ischemic brain injury in neonatal rats via inhibiting FUNDC1-mediated mitophagy. Acta Pharmacologica Sinica. 2024; 45: 1809–1820. https://doi.org/10.1038/s41401-024-01292-x.

[29] Gao Q, Zhu H, Dong L, Shi W, Chen R, Song Z, *et al*. Integrated Proteogenomic Characterization of HBV-Related Hepatocellular Carcinoma. Cell. 2019; 179: 1240. https://doi.org/10.1016/j.cell.2019.10.038.

[30] Gao Z, Sun W, Ni X, Wan W, Suo T, Ni X, *et al*. Low expression of RACK1 is associated with metastasis and worse prognosis in cholangiocarcinoma. Heliyon. 2024; 10: e27366. https://doi.org/10.1016/j.heliyon.2024.e27366.

[31] Goyal M, Demchuk AM, Menon BK, Eesa M, Rempel JL, Thornton J, *et al*. Randomized assessment of rapid endovascular treatment of ischemic stroke. The New England Journal of Medicine. 2015; 372: 1019–1030. https://doi.org/10.1056/NEJMoa1414905.

[32] Duehrkop C, Rieben R. Ischemia/reperfusion injury: effect of simultaneous inhibition of plasma cascade systems versus specific complement inhibition. Biochemical Pharmacology. 2014; 88: 12–22. https://doi.org/10.1016/j.bcp.2013.12.013.

[33] Huang J, Long Z, Jia R, Wang M, Zhu D, Liu M, *et al*. The Broad Immunomodulatory Effects of IL-7 and Its Application In Vaccines. Frontiers in Immunology. 2021; 12: 680442. https://doi.org/10.3389/fimmu.2021.680442.

[34] Marković I, Savvides SN. Modulation of Signaling Mediated by TSLP and IL-7 in Inflammation, Autoimmune Diseases, and Cancer. Frontiers in Immunology. 2020; 11: 1557. https://doi.org/10.3389/fimmu.2020.01557.

[35] Barata JT, Durum SK, Seddon B. Flip the coin: IL-7 and IL-7R in health and disease. Nature Immunology. 2019; 20: 1584–1593. https://doi.org/10.1038/s41590-019-0479-x.

[36] Yu J, Gadwa J, Ross RB, Knitz M, Darragh LB, Abdelazeem KNM, *et al*. IL7 in combination with radiotherapy stimulates a memory T-cell response to improve outcomes in HNSCC models. Cancer Immunology, Immunotherapy: CII. 2024; 73: 90. https://doi.org/10.1007/s00262-024-03664-y.

[37] Lei X, Cai S, Chen Y, Cui J, Wang Y, Li Z, *et al*. Down-regulation of interleukin 7 receptor (IL-7R) contributes to central nervous system demyelination. Oncotarget. 2017; 8: 28395–28407. https://doi.org/10.18632/oncotarget.16081.

[38] Zhao Z, Xue J, Zhuo Z, Zhong W, Liu H. The Association of *IL7R* rs6897932 with Risk of Multiple Sclerosis in Southern Chinese. Neuropsychiatric Disease and Treatment. 2022; 18: 1855–1859. https://doi.org/10.2147/NDT.S376066.

[39] Cui J, Wang H, Liu S, Zhao Y. New Insights into Roles of IL-7R Gene as a Therapeutic Target Following Intracerebral Hemorrhage. Journal of Inflammation Research. 2024; 17: 399–415. https://doi.org/10.2147/JIR.S438205.

[40] Cai S, Chen Y, Shang Y, Cui J, Li Z, Li Y. Knockout of zebrafish interleukin 7 receptor (IL7R) by the CRISPR/Cas9 system delays retinal neurodevelopment. Cell Death & Disease. 2018; 9: 273. https://doi.org/10.1038/s41419-018-0337-z.

[41] Michaelson MD, Mehler MF, Xu H, Gross RE, Kessler JA. Interleukin-7 is trophic for embryonic neurons and is expressed in developing brain. Developmental Biology. 1996; 179: 251–263. https://doi.org/10.1006/dbio.1996.0255.

[42] Zhang L, Duolikun M, Chen H, Wang Z, Li X, Xiao H, *et al*. Genome-wide KAS-Seq mapping of leukocytes in ischemia-reperfusion model reveals IL7R as a potential therapeutic target for ischemia-reperfusion injury. Scientific Reports. 2025; 15: 6165. https://doi.org/10.1038/s41598-025-90457-7.

[43] Yan M, Yang Y, Zhou Y, Yu C, Li R, Gong W, *et al*. Interleukin-7 aggravates myocardial ischaemia/reperfusion injury by regulating macrophage infiltration and polarization. Journal of Cellular and Molecular Medicine. 2021; 25: 9939–9952. https://doi.org/10.1111/jcmm.16335.

[44] Xu J, Liu X, Yu H, Wang Z. Tanshinone IIA inhibits the apoptosis process of nerve cells by upshifting SIRT1 and FOXO3α protein and regulating anti- oxidative stress molecules and inflammatory factors in cerebral infarction model. Immunopharmacology and Immunotoxicology. 2025; 47: 23–33. https://doi.org/10.1080/08923973.2024.2428662.

[45] Yao M, Liu Y, Meng D, Zhou X, Chang D, Li L, *et al*. Hydroxysafflor yellow A attenuates the inflammatory response in cerebral ischemia-reperfusion injured mice by regulating microglia polarization per SIRT1-mediated HMGB1/NF-κB signaling pathway. International Immunopharmacology. 2025; 147: 114040. https://doi.org/10.1016/j.intimp.2025.114040.

[46] Wei X, Guo H, Huang G, Luo H, Gong L, Meng P, *et al*. SIRT1 Alleviates Mitochondrial Fission and Necroptosis in Cerebral Ischemia/Reperfusion Injury via SIRT1-RIP1 Signaling Pathway. MedComm. 2025; 6: e70118. https://doi.org/10.1002/mco2.70118.

[47] Lindskog C, Edlund K, Mattsson JSM, Micke P. Immunohistochemistry-based prognostic biomarkers in NSCLC: novel findings on the road to clinical use? Expert Review of Molecular Diagnostics. 2015; 15: 471–490. https://doi.org/10.1586/14737159.2015.1002772.

[48] Bordoni V, Tartaglia E, Sacchi A, Fimia GM, Cimini E, Casetti R, *et al*. The unbalanced p53/SIRT1 axis may impact lymphocyte homeostasis in COVID-19 patients. International Journal of Infectious Diseases: IJID: Official Publication of the International Society for Infectious Diseases. 2021; 105: 49–53. https://doi.org/10.1016/j.ijid.2021.02.019.

[49] Dumbrava DA, Surugiu R, Börger V, Ruscu M, Tertel T, Giebel B, *et al*. Mesenchymal stromal cell-derived small extracellular vesicles promote neurological recovery and brain remodeling after distal middle cerebral artery occlusion in aged rats. GeroScience. 2022; 44: 293–310. https://doi.org/10.1007/s11357-021-00483-2.

[50] Przykaza Ł. Understanding the Connection Between Common Stroke Comorbidities, Their Associated Inflammation, and the Course of the Cerebral Ischemia/Reperfusion Cascade. Frontiers in Immunology. 2021; 12: 782569. https://doi.org/10.3389/fimmu.2021.782569.

[51] She R, Liu D, Liao J, Wang G, Ge J, Mei Z. Mitochondrial dysfunctions induce PANoptosis and ferroptosis in cerebral ischemia/reperfusion injury: from pathology to therapeutic potential. Frontiers in Cellular Neuroscience. 2023; 17: 1191629. https://doi.org/10.3389/fncel.2023.1191629.

[52] Guo H, Fan Z, Wang S, Ma L, Wang J, Yu D, *et al*. Astrocytic A1/A2 paradigm participates in glycogen mobilization mediated neuroprotection on reperfusion injury after ischemic stroke. Journal of Neuroinflammation. 2021; 18: 230. https://doi.org/10.1186/s12974-021-02284-y.

[53] Li X, Xie Z, Zhou Q, Tan X, Meng W, Pang Y, *et al*. TGN-020 Alleviate Inflammation and Apoptosis After Cerebral Ischemia-Reperfusion Injury in Mice Through Glymphatic and ERK1/2 Signaling Pathway. Molecular Neurobiology. 2024; 61: 1175–1186. https://doi.org/10.1007/s12035-023-03636-w.

[54] Fu D, Yan J, Zhang Z, Liu Y, Ma X, Ding J, *et al*. Nuclear PLD1 combined with NPM1 induces gemcitabine resistance through tumorigenic IL7R in pancreatic adenocarcinoma. Cancer Biology & Medicine. 2023; 20: 599–626. https://doi.org/10.20892/j.issn.2095-3941.2023.0039.

[55] Xue X, Wang H, Su J. Inhibition of MiR-122 Decreases Cerebral Ischemia-reperfusion Injury by Upregulating DJ-1-Phosphatase and Tensin Homologue Deleted on Chromosome 10 (PTEN)/Phosphonosinol-3 Kinase (PI3K)/AKT. Medical Science Monitor: International Medical Journal of Experimental and Clinical Research. 2020; 26: e915825. https://doi.org/10.12659/MSM.915825.

[56] Wang HJ, Ran HF, Yin Y, Xu XG, Jiang BX, Yu SQ, *et al*. Catalpol improves impaired neurovascular unit in ischemic stroke rats via enhancing VEGF-PI3K/AKT and VEGF-MEK1/2/ERK1/2 signaling. Acta Pharmacologica Sinica. 2022; 43: 1670–1685. https://doi.org/10.1038/s41401-021-00803-4.

[57] Li Y, Xia J, Jiang N, Xian Y, Ju H, Wei Y, *et al*. Corin protects H_2O_2-induced apoptosis through PI3K/AKT and NF-κB pathway in cardiomyocytes. Biomedicine & Pharmacotherapy. 2018; 97: 594–599. https://doi.org/10.1016/j.biopha.2017.10.090.

[58] Hou Y, Wang K, Wan W, Cheng Y, Pu X, Ye X. Resveratrol provides neuroprotection by regulating the JAK2/STAT3/PI3K/AKT/mTOR pathway after stroke in rats. Genes & Diseases. 2018; 5: 245–255. https://doi.org/10.1016/j.gendis.2018.06.001.

[59] Jing D, Wu W, Deng X, Peng Y, Yang W, Huang D, *et al*. FoxO1a mediated cadmium-induced annulus fibrosus cells apoptosis contributes to intervertebral disc degeneration in smoking. Journal of Cellular Physiology. 2021; 236: 677–687. https://doi.org/10.1002/jcp.29895.